REDVET - Revista electrónica de Veterinaria - ISSN 1695-7504
Vol 25, No. 1S (2024)
http://www.veterinaria.org
Article Received: Revised: Accepted:

Using a Lightweight Convolutional Neural Network for Contactless Multispectral Palm-Vein Recognition.

Komal Teotia[1*], Dr. Manav Bansal[2]

[1*] Scholar M.Tech CSE, SCRIET, Chaudhary Charan Singh University, Meerut, India
[2] Assistant Professor, SCRIET, Chaudhary Charan Singh University, Meerut, India

ABSTRACT:
Biometric recognition technology has advanced to the point of replacing traditional codes and credentials. One such technique gaining popularity is contactless palm vein verification, which is safe and sanitary. However, there are important issues to consider regarding system safety and scalability in deep learning (DL). Convolutional neural networks (CNNs) are among the most extensively studied deep learning algorithms, known for their ability to extract features. Nonetheless, training CNNs requires a significant intellectual effort and large sample sizes, resulting in higher hardware and software costs.To address the need for a substantial amount of palm-vein data, this research proposes to use a versatile Gabor filter with improved photographic characteristics and a triplet loss function.
This study used a multidimensional palm database from the CASIA accessible database to evaluate the suggested system. According to the study findings, the suggested approach only requires a small number of network configurations in a multispectral environment and has an average identification error rate of 0.0456%.

KEYWORDS: Biometric, palm-vein identification, convolution neural networks, triplicate loss function, handcrafted character.

1: INTRODUCTION

With the advancement of information technology, the field of information security has also made significant progress. Consequently, more and more laws and procedures have been developed to enhance the protection of personal data. Traditional measures of information security, such as passwords, smart cards, and identity cards, are often prone to being lost, forgotten, or stolen by malicious actors. The convenience, safety, and dependability that modern society demands are not met by these technologies. A novel approach based on distinct biological traits is thought to be the most efficient means of safeguarding personal data. For four key factors, biometric data—such as voice print, facial characteristics, fingerprints, fingers vein, palm print, and iris—can be used in place of codes for authentication of identity. First of all, biometric data is universal as each person has a unique set of biometrics. Second, genetic characteristics are irreversible because they rarely change significantly over time; instead, changes are small and uniform in nature. Lastly, biometric information is difficult to forget, making it highly secure.Every person has distinct biological characteristics that are different from others. Even identical twins have unique palm-vein information. This uniqueness is known as distinctiveness. Genetic information can be collected promptly and expediently using unique instruments. This is known as collectability [1].
Compared to standard identity documents or credentials, genetic data about the human body is a more secure, dependable, and practical way of authentication. This knowledge is not easily neglected, is not as able to be taken away, and may be utilized to swiftly and effectively authenticate someone's identification. Biochemical characteristics can be divided into two categories: internal traits found within the body, such as the wrist vein, palm vein, dorsal vein of the hand, and finger vein; and external qualities found on the exterior of the human body, such as the face, iris, and palm print. Table 1 illustrates how effortlessly fingerprints and face features—both exterior traits—can be taken and utilized by unauthorized people.
Furthermore, since fingerprints are less comprehensive than facial traits, they aren't secure.

Features	Taken	Security	Isolation	Comfort	Hygiene
Face	RGB	Middle	Low	High	Low
Iris	NIR	High	High	Low	High
Fingerprint	Press optic	Middle	Middle	Middle	Low
Palm-vein	NIR	High	High	High	High

Over time, iris recognition gets uneasy because knowledge is captured by nearinfrared (NIR) light. People have been obliged to limit physical contact as a means of preventing the spread of the COVID-19 pandemic. These two approaches have become unsanitary and inconvenient since they require users to touch a sensor's surface for finger print recognition and remove face masks for facial recognition. An essential characteristic, the palm vein, appears more appropriate and relevant given the status of the globe today. The palm vein is sturdy and difficult to mimic since it is inside the person

body; also, ordinary stains and injuries do not interfere with detection. Even between twins, the vein is remarkably distinct and does not alter much over time.

A palm-vein image depicts the vein network beneath the skin of a living human; this vein network is invisible to the naked eye and can only be imaged using near-infrared radiation (NIR) that is immersed by hemoglobin in the blood. Muscles that refract light provide an NIR spectrum that spans from 750 - 1050 nm [10]. Because users do not have to interact with the detector during recognition, authentication using the palm vein has proven to be more successful than that using other biological characteristics [1], [11]. Additionally, the knowledge gained through this method cannot be gathered intentionally or by illegitimate ways. We make reference to the relevant studies [1], [46], and [50] and list in Table 1 the benefits and drawbacks of the different identification techniques.

As the palm vein may only be detected by presenting the fingertips to NIR light, collecting samples for deep machine learning (DML) model development is difficult. When compared to conventional methods, DL uses superposition to find the best features, which works better with larger datasets. Over the past several years, hardware has become faster and faster. Lightweight neural network computing is now possible thanks to the presence of CUDA parallel computing modules in many embedded devices. Edge computer systems are predicted to become much more popular as long as equipment costs keep falling.

In order to fully segment the hand shape, traditional recognition algorithms have primarily been verified utilizing publicly accessible datasets with a straightforward database backdrop. Nevertheless, interference might happen and hand movements, rotations, or magnification could affect recognition; these issues obviously need to be fixed (Fig. 1). Ultimately, it is anticipated that various devices will record varying vein image spectra and that these variations will affect how adaptable their systems are. Therefore, a model that can adapt to various spectra needs to be created.

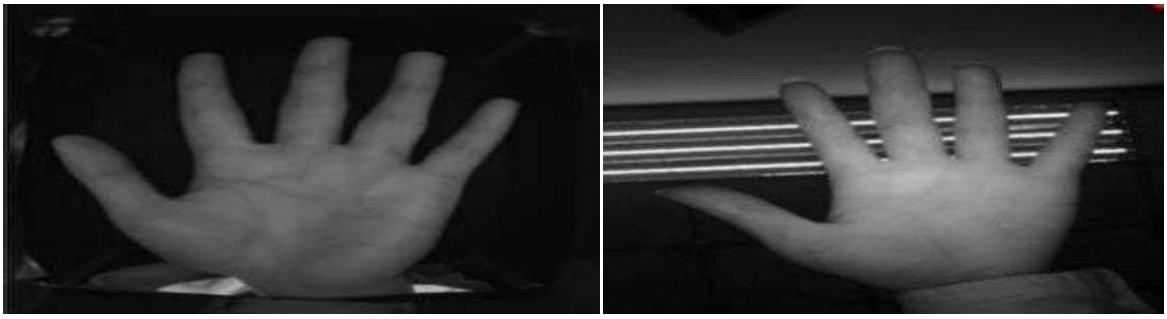

Figure 1: Interference with palm images: (a) the publicly available dataset is interferencefree. (b) An interference-filled actual image.

2: LITERATURE REVIEW

Vein-based authentication methods have gained a lot of interest in recent years. These techniques include palm-vein [1], [4], [7], finger-vein [5], [6], [12], dorsal hand vein [8], wrist-vein [9], and forearm vein [14]. Palm-vein identification is selected the same as the research topic for this work because it is thought to be the most practical of these due to its numerous properties and ease of capture. The conventional palm vein identification system in Fig. 2 primarily uses NIR cameras to capture images. After extracting the region of interest (ROI) and matching the derived characteristics and locations with those in the database, the generated images are examined. On the other hand, system efficiency is directly impacted by the feature gathering technique. There are two types of features in the present palm vein identification system: CNN-based characteristics and handmade characteristics. To obtain characteristics from handcrafted items, there are three methods available:

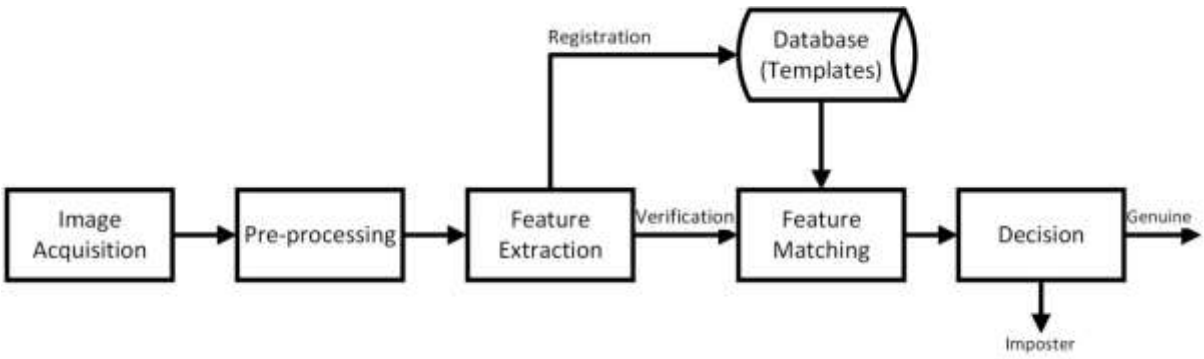

Figure 2: The palm vein identification system flow.

A): The technique which is based on geometry [7], [15] primarily utilizes vein texture to represent a connected linear creation within the picture. It effectively gathers data regarding lines, curves, and points that closely resemble the texture and shape of veins. However, this approach requires rectification throughout ROI initially; with the extracted features often appear unclear or meagre. Consequently, it becomes challenging to handle samples that undergo rotation, scaling, or displacement.

B): Using information from statistics, the statistical-based technique [16] finds picture properties like picture unchanging instances and localized digital histograms. Local statistics, which include local binary structures (LBS) and local derivative structures (LDS), can be applied to the latter [17]. Alternatively, full-range information, which entails picture consistency, may also be applied [18]. Nevertheless, these methods display inconsistency when users' hands rotate, scale, and shift.

C): Home invariant palm-vein features can be easily extracted using a home invariant-based technique [19], which draws inspiration from the scale invariant feature transforms (SIFT) algorithm used in traditional computer vision (CV). While it can compensate for the effects of hand rotation and feature displacement, it is vulnerable to variations in the light source within the apparatus or surroundings. It can therefore recover more reliable characteristics, which reduces its effectiveness as a detection method.

DL has become widely utilized in various fields due to the decrease in hardware costs and the improvement of computing power. Previous research suggested the utilization of PVS Net [20] and handcrafted features as the training target. This was achieved during a well-made auto encoder, CNN, where the determined descriptions were then passed through completely associated layer. Users' confirmation was established using a categorization network. However, the use of handcrafted features eliminates DL's ability to find the optimal solution on its own. In a different study, Badalona et al. [13] proposed a combination of the binaries arithmetical picture feature descriptor process and CNN approaches. They employed a decision-level mixture scheme for palm-vein acknowledgment systems, focusing solely on identification in their experimental analysis. Another study by Das et al. [21] introduced a CNN structure for finger-vein, aiming to attain pictures of the similar superiority. Widespread experiments were conducted to demonstrate its usefulness.

Nonetheless, this approach yields categorization outcomes directly. Consequently, every time a user was enrolled, the network needed to undergo retraining, necessitating a significant figure of parameters. Fang et al. [22] introduced a streamlined network configuration to assess the entropy and multiple ROI of finger-vein images, integrating it with a two-stream network for categorization authentication. Nevertheless, the data used for guidance and trying were sourced from pictures captured simultaneously, a practice deemed unsuitable due to the possibility of slight, unpredictable alterations in real data throughout every analysis. It is crucial to make sure that the guidance and trying data are gathered at dissimilar time intervals to showcase the algorithm's resilience.

The majority of the existing palm-vein acknowledgment systems still possess certain limitations. For example, traditional algorithms require numerous modifiable parameters, which significantly prolong the time needed to attain higher accurateness based on user knowledge [44]. Additionally, some algorithms only utilize a portion of the available data during experimentation, leading to an increase in error rates as the number of users grows [7]. Furthermore, present DL-based algorithms encounter various challenges, such since the extensive data requirements of CNNs and the risk of over fitting datasets. Moreover, the palm-vein database accessible to the public is smaller compared to the finger-vein database, and the numeral of photos that can be captured for each user is insufficient. Consequently, the development of DL in palm-vein recognition lags behind that of finger-vein recognition. Nonetheless, this document concentrates on palm-vein recognition, which offers additional distinctive characteristics and enhanced security compared to finger-vein acknowledgment.

3: SUGGESTED METHODS

The palm-vein identification scheme depicted in Figure 3 was urbanized using earlier research and CNN. It comprises of 2 components: guidance and testing. Initially, the ROI process was employed to determine the specific area for identification. The ROI picture and Gabor filter be then utilized to calculate the convolution and

REDVET - Revista electrónica de Veterinaria - ISSN 1695-7504
Vol 25, No. 1S (2024)
http://www.veterinaria.org
Article Received: Revised: Accepted:

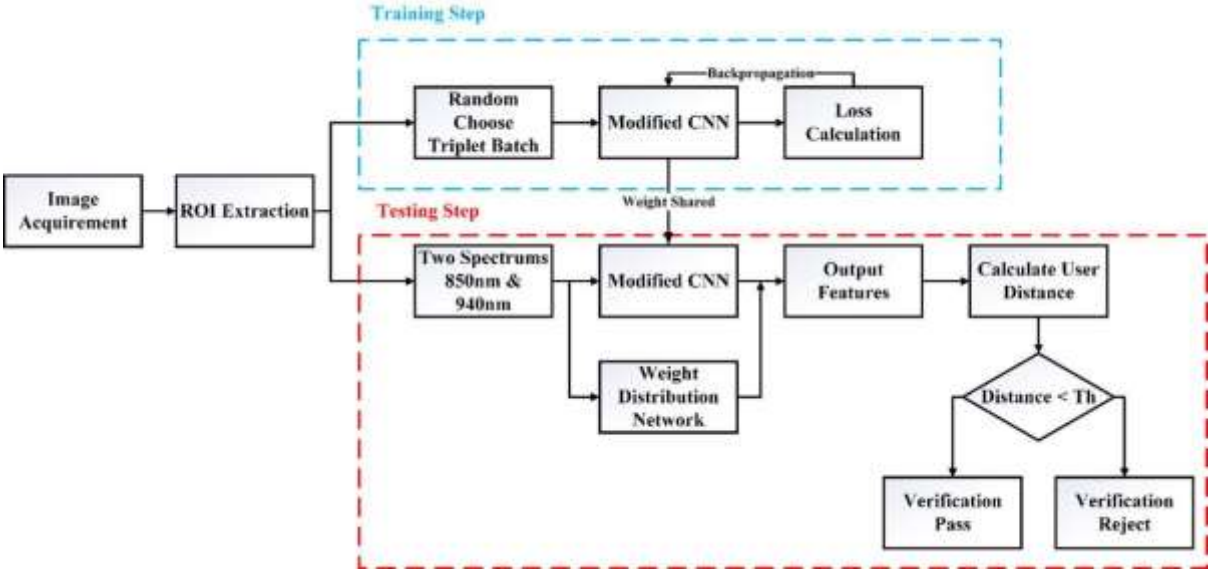

Figure 3: suggested architectural design.

Take out the relevant description. During the deep network guidance stage, input mixture was conducted among the original ROI picture and Gabor character. Subsequently, triplet loss and cross entropy were computed to optimize the deep network weight during back propagation (BP) when the after that consignment of deep network guidance was performed.

A. SYSTEM FLOWCHART

A weight selection mechanism was introduced in this study to determine the optimal image in a dual spectrum. The chosen sample was assigned a higher weight during the succeeding corroboration process, which utilized the Euclidean distance. If the distance among the tough and registered data fell under the entrance, the user's in sequence was deemed accurate. However, if the distance exceeded the threshold, the user's in sequence was deemed unreliable.

B. POSITIONING ROI

All information, apart from for the preferred veins, is considered unimportant. Therefore, an effective background subtraction algorithm is necessary to enhance the performance of the system. Biometric information can be obtained using moreover contact or contactless strategy. While the dislocation of contact devices can be minimized through physical settings, contactless devices are seen as the future mainstream option because users do not need to physically touch them, making them extra sanitary [1]. However, contactless strategies tend to produce additional invalid results due to variations in palm size, hand dislocation, and revolution between different images captures. Hence, several algorithms were employed in this study to ensure that the captured palm-vein information remained unaffected by these issues. In Figure 4, the practical approach involved utilizing semantic image segmentation (Deep Lab V3C) for background subtraction prior to capturing the palm image. Subsequently, the radial distance function (RDF) was employed to identify the fingertip and finger valley by measuring the distance between the orientation point and the outline point. Following this, the foreground details were extracted based on the hand amount and revolving improvement direction. The specific procedures are outlined below:

(a) (b) (c)

REDVET - Revista electrónica de Veterinaria - ISSN 1695-7504
Vol 25, No. 1S (2024)
http://www.veterinaria.org
Article Received: Revised: Accepted:

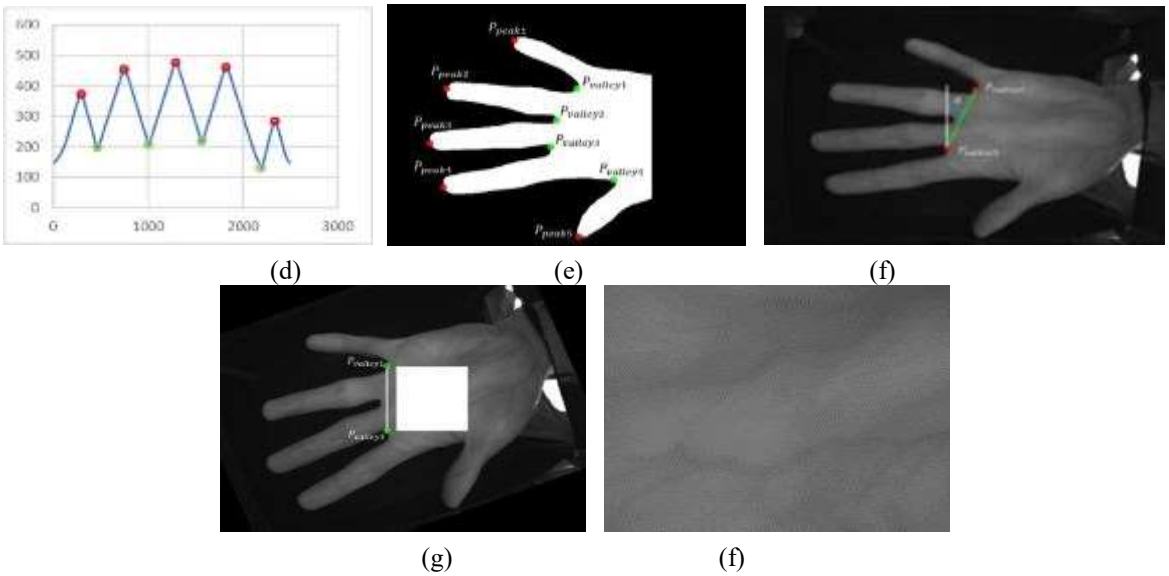

Figure 4: The original vein image is the ROI point for the palm-vein capture.(b)

Picture of binary. (c) Centers of bars and defined references. (d) RDF.(e) Identified valleys and finger tips. (f) Rotation angle computation (g) Image normalization.(h) ROI picture.

1) PALM CONTOURING

The conventional approach contours the palms using grayscale photos after accurately extracting ROI images. Unfortunately, because of the fluctuating ambient light, it is unable to extract reliable background and foreground information. The palm picture in this study was segmented in front of the backdrop using Deep Lab V3C [23], [49]. As seen in Fig. 4(b), the network that had been trained successfully separated the forefront palm from the backdrop disturbance illumination resource. Consumers frequently wear items like clocks and ornaments, which are typically linked to the palm and cannot be detached through the contouring segmentation, according to the real examples that were acquired. As can be seen in Fig. 4(c), the authors first determined the location of the BaryCentre within the picture, then predictable the parallel distance L (which is a variable parameter made up of the hand image's center of gravity and the location of roughly 0.8 palm dimensions from left to right), and finally removed the portion so as to exceeded the extent L. This technique successfully eliminated hand disturbances and increased the structure's reliability.

2) INDICATING THE VALLEYS AND FINGER-TIPS

Next, the locations of the basins and fingertips are determined. To erive the RDF, the European distance between the mass centre and the hand contour was computed, using the barycentre (P_{ref}) of the hand contour as the reference point (see Fig. 4(c)). The hand contour image's valleys (Pbasins1 to Pbasins4) and fingertips (Ppeak1 to Ppeak5) were found to be located in five places of greatest rate and 4 areas of lowest rate, respectively (see Fig. 4(d)).

3) NORMALIZATION AND ROI EXTRACTION

As shown in Fig. 4(e) and in Equations 1 & 2, where xPbasins1 & xPbasins4 represented related coordinate, the writer used Pbasins1 and Pbasins3 as orientation points, denoted d to characterize the smallest distance among two regard points, and used θ to correspond to the position among the straightline d and the at right angles line. Furthermore, bilinear interpolation was used to rectify the palm angle. After adjusting the two reference points in Fig. 4(g), the double palm-vein picture was taken, as seen in Fig. 4(f) $d = \sqrt{(xp_{basin1} - xp_{basin3})^2 + (yp_{basin1} - yp_{basin3})^2}$ (1)

$\theta = \tan^{-1}(xP_{basins1} - xP_{basins3}) / (yP_{basins1} - yP_{basins3})$ (2)

C. ADJECTABLE GAP FILLERS

The Gabor filter is a popular characteristic withdrawal technique that has been used in many different domains due to its outstanding effectiveness in frequency examination and feature extraction, as demonstrated by Eq. 3. It is useful for studying particular frequencies. Five distinct characteristics are used to fine-tune the gabor restrictions, giving them a great deal of flexibility to adjust to an array of data. Testing various configurations is necessary to identify the most

appropriate settings. In order to increase the filter's flexibility, this study used a two-dimensional Gabor filter with self-adapted distinctiveness.

$$I_{\square\square\square\square,,}\square g\,x\,y(\ ,\ ).\sin[2\square\square\ \square\ \square\square x\cos\ \square y\sin\ \square] \quad (3)$$

By limiting the number of variables to those that significantly affect the preserved vein sample, the 2D Gabor filter was made simpler. The following is the modified equation:

$$G\square\square\square,\ ,(x\ y,\ )\ \square\ g\square(x\ y,\ ).\exp(2\square\square\ \square j\ (x\cos\ \square\ y\sin\ ))\square \quad (4)$$

In Eq. 4, j denotes the imaginary unit and $g\_\ (x; y)$ is further expanded in Eq. 5.

$$g_{\square}(x\ y,\ )\ \square\ \frac{1}{2\square\square_{2}}\ .\exp\square\ \square\ \frac{\square\square\square x2\ \square\ y2\square\square}{2_{\square}2}\ \square_{\square} \quad (5)$$

Where μ represents the sample's central frequency, σ stands for the major angle, and σ represents the standard deviation (SD).

Real and imaginary component functions were further separated from the 2 Dimensional Gabor filter in Eq. 4. The imaginary part function was utilized for border recognition and the real part function for vein saddle recognition. Gσ,μ,θ was broken down using Euler's formula to provide the real part Rσ,μ,θ and the imaginary part Iσ,μ,θ.

$$R_{\square\square\square\square,,}\square g\,x\,y(\ ,\ ).\cos[2\square\square\ \square\ \square\square x\cos\ \square y\sin\ \square] \quad (6)$$

$$I_{\square\square\square\square,,}\square g\,x\,y(\ ,\ ).\sin[2\square\square\ \square\ \square\square x\cos\ \square y\sin\ \square] \quad (7)$$

When the 2D Gabor filter's parameters σ, μ, and θ are in harmony, the most effective results may be achieved [24]. The initial palm-vein picture was divided into several sub regions using a dynamic variable in this study, and the optimum value for each sub region was then found. However, owing of the intricate natural vein structure, it is difficult to use defined parameters to palm-vein identification because the outcomes vary from collection to collection.

1) STANDARD DEVIATION OF FILTER

In this learn, σ stood for the Gaussian distribution's standard deviation. The value of this variable changed the filter's envelope length. On the other hand, an insignificant amount of σ obtains more texture detail; a great rate of σ makes the filter extra resistant to intervention [25]. To determine the filter settings appropriate used for the palm-vein picture in the research, we referred to [27]. Using equations (8) and (9), the SD of the sub area is determined, and equation (10) yielded the optimal sigma variable.

$$F\,I\,i\,j\square\ \square\ ,\ \square\square\square\square\square i\square 1\ \frac{\overset{m}{\underset{j\square 1}{n\,I\,i\,j\square\ ,\ \square}}}{m\ n\square} \quad (8)$$

()

$$\square\ \square_{i\square 1}\ \overset{m}{\underset{j\square 1}{n}}\square I\,i\,j\square\ ,\ \square\square E\,I\,i\,j\square\ \square\ ,\ \square\square\square^{2} \quad (9)$$

$$D\,I\,i\,j\square\ \square\ ,\ \square\square\square\ \sqrt{\frac{}{m\ n\square}}$$

Where E ($I_{(i, j)}$) denotes the signify rate of the sub-region, and D($I_{(i,j)}$) denotes the SD of the sub region.

The four variables in Eq. 10 represent the stable zone, slow zone, moderate zone, and rapidly changing zone respectively, which better fit most of the samples.

$$\begin{array}{l}\square 1,if D\,I\,i\,j\square\ \square\ ,\ \square\square\square 1\quad\square\\ \square\square\\ \square\square\ 2,if 1\square\ D\,I\,i\,j\square\ \square\ ,\ \square\square\square 1.4\quad\square_{\square}\\ \square\square\square\square\\ _{\square}22,if 1.4\ \square\ D\,I\,i\,j\square\ \square\ ,\ \square\square\square\ 2.8_{\square}\\ \square\square\\ \square_{\square}42,if D\,I\,i\,j\square\ \square\ ,\ \square\square\square\ 2.8\ \square_{\square}\end{array} \quad (10)$$

2) CENTER FILTER REGULARITY

The gray level shift in the primary direction can be evaluated as a sinusoidal waveform in order to determine the range T among the smallest or maximum levels in both regions. Using this method, one can also determine the center frequency μ by using the formula μ = 1/T. It was challenging to identify the boundary areas since the contrast between the muscle tissue and veins in the experiment's samples was not as strong as it was in a natural image [26]. To get a higher system performance, additional techniques were required to get a representative value of μ. We suggested dividing μ into four ranges in our investigation, each of which matched one of the 4 SDs. Following investigational examination, it be discovered so as to a greater rate of SD and a lesser rate of T on the vein suggested that the picture included more intricate consistency elements. As a result, we may calculate the necessary using SD.

□0,*if*□□1 □
□0.12,*if*□□ 2
□□□
□0.8,*if*□□ 2 2 (11)
□□2,*if*□□ 4 2

3) FILTER MAIN ANGLE

The major direction of this segment was ascertained by analyzing the textural properties of each sub region that was created when the vein image was divided into multiple smaller ones. First, the greatest angle of every pixel is found in Eq. (12), and the gradient variations of the effort sub regions were recognized in both the upright and parallel directions.

$$\square \qquad 1\ dy\ i\ j\square\ ,\ \square\ I\ \square i\ j,\ \square\square\ \tan\square\ \frac{\qquad\qquad}{dx\ i\ j\square\ ,\ \square} \qquad (12)$$

To minimize the calculation load, the angles were separated into 6 primary angles for the purpose of figuring out every pixel's angle. Six main angles, according to [27], can be used to achieve a balance between computation and performance. To preserve the optimal resolution for every angle during the angular segmentation process, a linear difference was employed. Eq. 13 yielded the maximum major angle in the sub region.

$$\square\square \arg\max\square \sum_{\square\ \square_{xo}\square_1}^{n} \sum_{yo\square_1\ \square\square}^{m} I\ \ i\ j, \qquad (13)$$

The ideal filter parameters, σ, μ, and θ, were found for each sub area by utilizing the angular order ϕ ε {00, 300, 600, 900, 1200, 1500}. These parameters further divided into real portion CRσ,μ,θ(i,j) and imaginary part CIσ,μ,θ(i,j). Lastly, the real and imaginary parts of the Gabor filters belonging to each sub region were complicated. According to Eq. 14, the picture was transformed with eigenvalue after inversion.

$$F_R\ \square i\ j,\ \square\square\square \begin{cases} \square_{\square}1,if CR_{\square\square\square,,}\ \square i\ j,\ \square\square\ 0 \\ \square_{\square}0,if CR_{\square\square\square,,}\ \square i\ j,\ \square\square\ 0 \end{cases}$$

$$F\ i\ j_I\square\ ,\ \square\square\square \begin{cases} \square_{\square}1,if CI_{\square\square\square,,}\ \square i\ j,\ \square\square\ 0 \\ \square_{\square}0,if CI_{\square\square\square,,}\ \square i\ j,\ \square\square\ 0 \end{cases} \qquad (14)$$

D. MODIFIED CONVOLUTION NEURAL NETWORK

Following pre-processing and normalization of the palm-vein pictures, the outcomes were fed into an upgraded CNN. In the following stage, the input data was converted using CNN into an embedding characteristic for user justification. When compared to the most current DL-based palm vein acknowledgment, the following are the benefits of this study:

(1) *Image feature derecognition*: A number of classifiers are used inside the majority of palm vein acknowledgment systems that are now in use when paired with deep learning [21], allowing for rapid identification. It is of little utility for real-world applications that the network must be tuned once more in order to accommodate more users [37]. By moving the input picture into establishing features and compare the characteristic distance between the analysis data and the record information during verification, the suggested solution was able to get around this problem. It may, however, because a delay in the guidance series, as the entrance rate may be established for retention based on real-world scenarios. As a result, it's imperative to prevent the circumstance where new users require quick training.
(2) *Resolving the issue of not enough information resulting from limited sample sizes*: Deep learning (DL) has the potential to be highly efficient in the recognition of natural photos, but it needs a huge number of pictures to instruct a robust weight, which is a significant drawback for minute databases. Three samples of each kind are allowed for training because to the scarcity of the palm-vein database. In light of this, the learn improved the filter's features and included 3-triple loss along with its unique data arrangement to address the issue.
(3) *Developing lightweight system architecture designed for vein images*: Large network frameworks require numerous processing periods in order to fully train the system using the DL approach.
Convolution and fully-connected layers make up the majority of the CNN framework's parameters and computing time. The general convolution layer in biometric systems is sometimes replaced by a depth wise separable convolution layer, as suggested by Sandler et al. [29] for low-end embedding devices that are unable to perform large computation volumes. In order to reduce the weight of the network structure, the global average pooling (GAP) method flattened feature pictures and connected them with neurons.

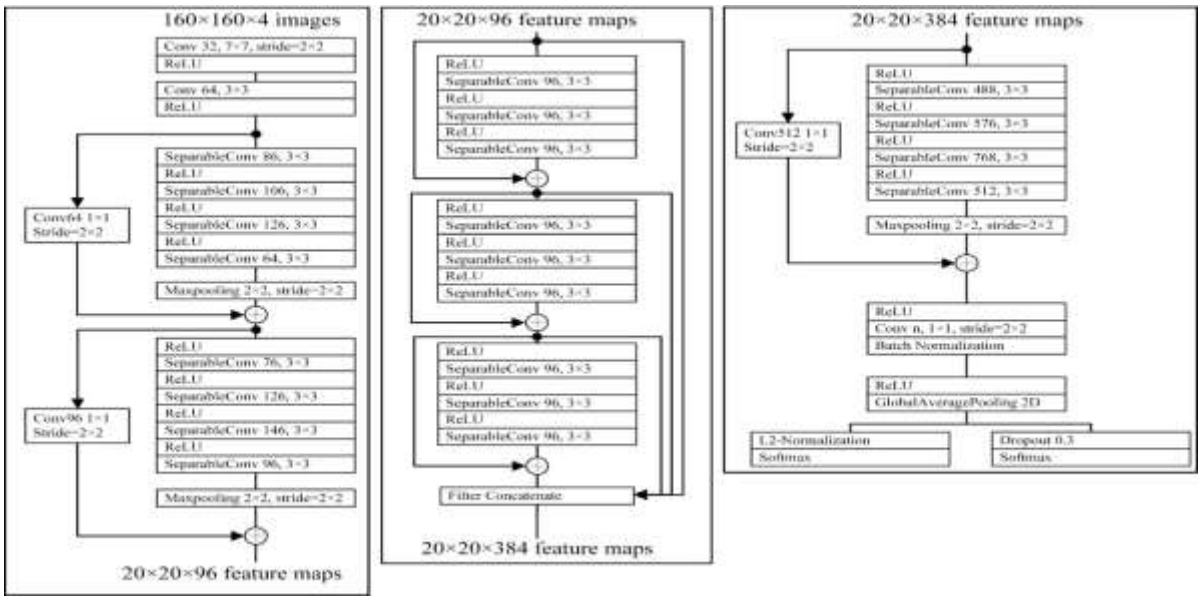

FIGURE 5. The CNN framework that has been modified and proposed. **1)**

NETWORK FRAMEWORK DESIGN

The suggested modified CNN framework, as seen in Fig. 5, was made up of eight modules and 27 convolution layers. All of the modules, with the exception of the input and output modules, employed residuals to transfer data amongst themselves. In order to prevent the frequent issues of excessive fitting and inner covariate shift in DL, a batch of normalization (BN) layers following the convolution level and a withdraw level before the output have been included in this study. As a result, the input level, middle level, and production level were the three main layers that were produced.

A: INPUT LAYER

In order to prevent the scale conversion from reducing the amount of information about the texture of the palm vein, the input data layer's size was changed to 160 ×160×4. Additionally, this made input fusion possible, enhancing the effect of feature fusion. A standard convolution layer with a big filter was the first input layer module. It was used to gather more valuable characteristic information, which was subsequently sent to the next system. Ultimately, each element within the input level employed a sub-sampling layer to decrease the dimension, resulting in the transformation of the original 160×160×4 picture into a 20× 20× 96 characteristic plot.

REDVET - Revista electrónica de Veterinaria - ISSN 1695-7504
Vol 25, No. 1S (2024)
http://www.veterinaria.org
Article Received: Revised: Accepted:

B: INTERMEDIATE LAYER

The input features were 20 × 20 × 96 in size after characteristic taking out and sub sampling in the input level. Since many tiny volume layers are functionally similar to one huge volume level but require fewer parameters, this study used minor convolution cores for several convolutions [30]. Three tiny blocks made up the intermediate module, and each block connected to a residual. The gradient disappearance issue was fixed by connecting the modules via a dense block, which also served to highlight feature reuse and maintain the best feature information. Following the module connection, the production feature plot measured 20 × 20 × 384 pixels.

C: OUTPUT LAYER

In order to incorporate the features as of the middle method and optimize the production that was produced in this level, a feature extraction component was initially linked. This module compacted the data using a 1×1 volume level after enlarging the feature map from 20 ×20×384 to 20 ×20×512. The output neural cell among them was designated by the shield number n, and its quantity was scaled in accordance with the various database sizes, with the least quantity being greater than the required minimum of users. Subsequently, the characteristic map was computed from a range of 20×20×n to n nerve cell using the GAP layer. Then, the n neurons underwent L2Normalization.Since the BN layer can smooth out characteristic variances and provide undesired image features as output, it was not used.

2) TRIPLET LOSS FUNCTION

It is crucial for the palm-vein identification system's network learning to be able to independently measure the similarities between the input photos. In order to provide input to the neural network for mass updates, this study used a triplet loss occupation that might determine the inter-sample comparison in concurrent throughout network teaching. The primary objective of deep networks is to train models capable of identifying similarities between images. The capacity of the triplet loss occupation to move the anchor away from the negative trial and to condense the distance among it and the positive trial is its most significant feature. A user's image is chosen as the anchor in Figure 6, and additional pictures of the similar user are chosen as the positive trial. A picture from one of the other users is chosen as the negative trial. Up until each sample is entered as an anchor in the database, the data is bringing out in this order. Upon traversing the levels, the image of the palm vein will change to become embedded. Prior to using the squared Euclidean distance to verify the comparison between two embedded characteristics, we distinct two palm-vein pictures, A and B.

$$D\,f A\square\ \square\ \square, f B\square\ \square\square\square \| f A\square\ \square\square f B\square\ \square \|22 \qquad (15)$$

Where D (.,.) stands for the square of the Euclidean distance in space and f is the function for mapping the picture to the embedding level.

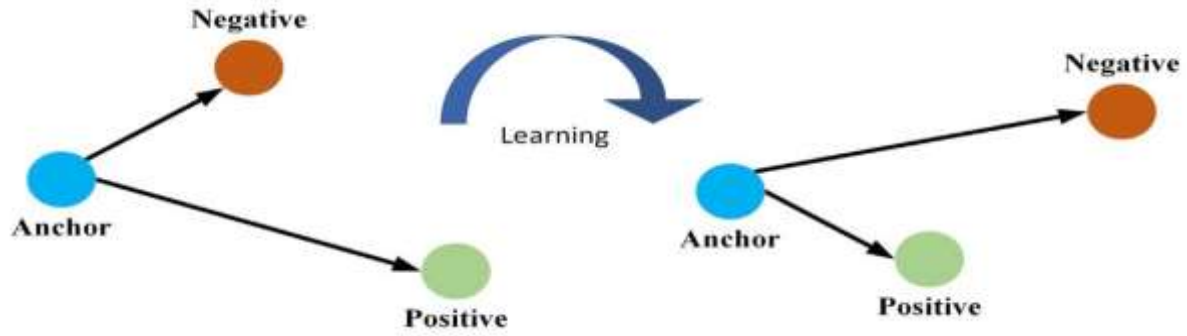

FIGURE 6. Three-fold loss function learning process.

The similarity between the original images A and B will increase with the distance of D (A, B). The positive and negative examples were identified using the information from the anchor as a collection of triplets bi = (pi, pi6+, pi-), with pi, pi+ represent the same user but different photographs, and pi- represents an image of a different user that is chosen at random until all images have been sorted as an anchor. The triplet loss function was calculated by Eq. 16 applying the squared Euclidean distance for merging the triplet and researching other loss type categories [31]. In this case, t is the gap variable that adjusts the two comparative pictures (p_i, p_i+) and (p_i, p_i-).

$$loss\ pi\ pi\square\ ,\ \square, pi\square\ \square\square\ \max 0,\square\ t\ \square D\,f\,pi\square\ \square\qquad \square, f\,pi\square\ \square\ \square\square\ D\,f\,pi\square\ \square\qquad \square, f\,pi\square\ \square\square\square\ \ (16)$$

Unlike traditional methods that rely on handcrafted features, DL was used to learn from the sample itself to identify the key characteristics for similarity judgment based on the previously mentioned loss function. As seen in Fig. 7, a batch of photos that CNN had extracted was entered during training. Images pi, pi^+, and pi^-were simultaneously transformed into embedding features from 2D images. After computation, the standard of the loss function was determined using Equation 16. The loss rate received as of each batch was utilized to optimize the CNN's weight using the BP approach, while the standard loss rate was employed to avoid excessive examples from impairing network learning.

REDVET - Revista electrónica de Veterinaria - ISSN 1695-7504
Vol 25, No. 1S (2024)
http://www.veterinaria.org
Article Received: Revised: Accepted:

E. MECHANISM FOR DOUBLE PICTURE WEIGHT SELECTION

According to earlier research, water absorbs light with wavelengths of 965 nm, while oxygenated and unoxygenated haemoglobin in person blood attract light with wave numbers between 750 and 1050 nm [6, 7, 10, and 11]. Not all vein images in real vein data perform better in the presence of light at the optimal wavelength for an absorption rate of 850 nm. Additionally, a number of circumstances, such as the equipment being used or the user's physical state at the moment of image capture may have an impact on users, potentially leading to conflicting data under the same spectrum.

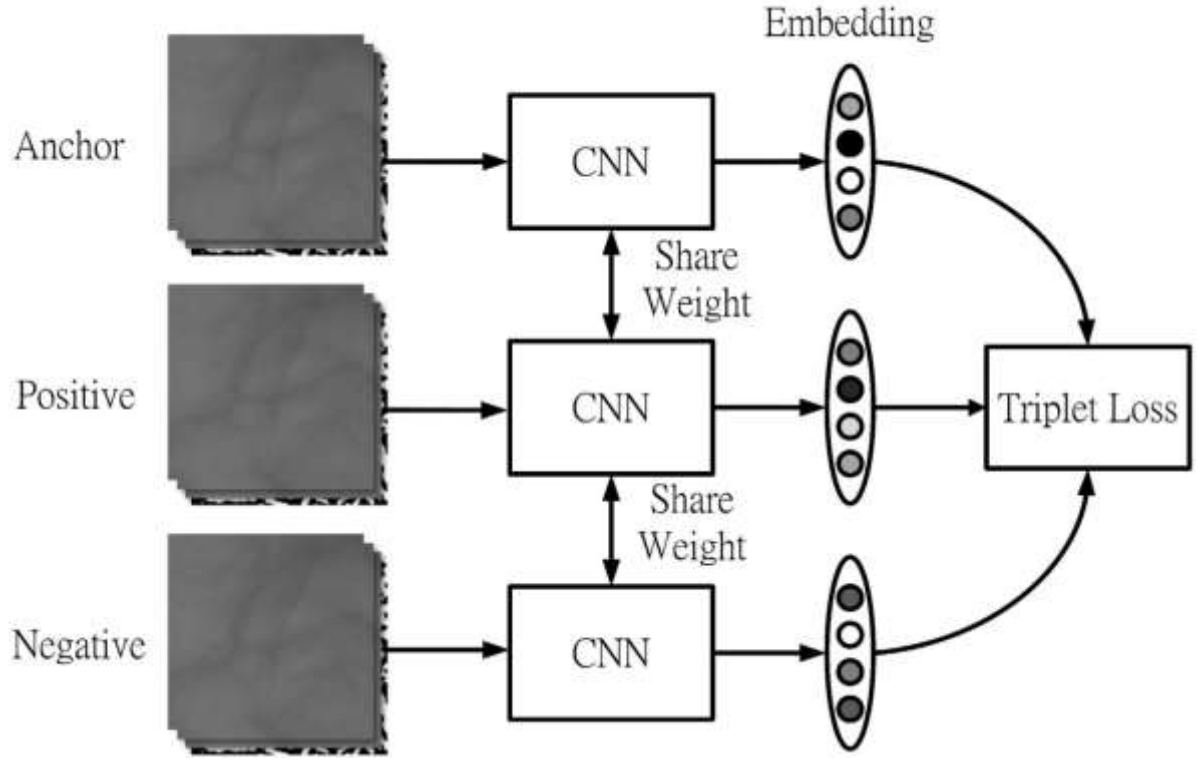

FIGURE 7. Training of the triplet loss operates system.

This research used a weight selection process to automatically identify the optimal spectrum for each user-taken multispectral image in order to overcome this challenge.

We cross-check the training data to determine the relative distance relationship b/w the samples, which allows us to describe the distance relationship b/w the pictures. Pair 850 nm and 940 nm measurements, then use Eq. 17 to construct a train tag. Lastly, the same neural network structure used for the input layer is used to choose the neural network's weight.

{Distance 850nm equal distance 940nm, α=01, β=01
{Distance 850nm great than distance 940nm-gap, α= 01, β= 0
{Distance 850nm less than distance 940nm-gap, α= 0.650, β= 0.350
{Distance 940nm great than distance 850nm-gap, α=0, β= 01
{Distance 940nm less than distance 850nm-gap, α= 0.350, β= 0.650 (17)

The constraint of α and β represent the label value assigned to the dissimilar wave numbers.

4. RESULTS AND ANALYSIS

A. ENVIRONMENTAL

The multiband palm databases CASIA [32] & PUT [38] were worn to assess the technological objectivity reported in this work. First, 7,200 photos taken with a contactless device were made available by a CASIA database. A total of one hundred users' right- and left-hand images were collected. The samples were gathered in two sessions, separated by a month. Every time, three pictures were taken, and six samples were concurrently recorded at various wave numbers (460, 630, 700, 850, 940 nm, and white). The writer examined the vein data that was taken between 850 and 940 nm in wavelength.

To do additional comparisons between the distinct samples, the image on the left and the image on the right. Of the same individual were regarded as pictures from separate users, increasing the number of subjects to 200 and each photograph to 12 users. Data testing in session 1 and training in session 2 provide information. Secondly, 1,200 contact device-captured photos were made available by a PUT vein database. Left- and right-hand visuals from a total of 50 users were obtained. The specimens were gathered over the course of three sessions, separated by one week. Four Every time, pictures were taken, and 880 nm samples were placed under fixed wavelengths and recorded concurrently.

Items	Specifications
CPU	Intel ® Core ™i7-6700@3.4GHz
Memory	DDR4 32GB
Graphics	Nvidia Geforce RTX 2080 Ti @1770MHz
Operating System (OS)	Microsoft Windows 10
Programming Language	C++,Python
Software	Tensorflow 1.10.0, Keras 2.24,OpenCV 3.4.3

The left and right photographs of the same individual were treated as images from distinct users in order to allow for additional comparisons between the samples. This increased the number of subjects to 100, with 12 pictures per user. The training sessions 1 & 2, as well as the data testing session 3.

In this work, algorithms were developed using Keras and OpenCV. Table 2 displays the specifications in detail. After building the data structure for triple for teaching, every sample occupied the anchor. 18 negative samples and 4 positive samples were coupled with a single anchor, yielding 86,400 triplet loss datasets in total. Following that, the network was fed these for a period of time before starting a fresh cycle of dataset for triplet loss development. With a batch range of datasets for six triplet loss and a learning rate of 0.001, the optimizer employed Adam.

The equal error rate (EER) confirmed the biometric system's security evaluation. The two possible error patterns that the system may encounter are the false reject rate (FRR), which suggests that the examiner must have completed the verification stage, and the false acceptance rate (FAR), which shows that the false tester wasn't supposed to pass the test. Modify the system's threshold such that FAR and FRR gradually approach 1 from 0 and 0 from 1, respectively, as protection is gradually reduced from a high to a low stage. The two data will ultimately converge at the same location in this process, which is known as EER. This is the point at which the system's performance is optimally balanced. The FAR and FRR definitions are presented in Equation 18. The device operating characteristic graph (ROC) was employed in addition to EER. The true acceptance rate (TAR), which was locate as the yaxis, was obtained by reversing the False Reject Rate, and the false acceptance rate was locate as the x-axis. In a straight line with an angle of one was set at the same moment. The algorithm's EER point was the point where the curves formed by false acceptance Rate and False Reject Rate intersected on a line segment with an angle of 1.

False Acceptance rate =FP/ (TN+FP)
False Reject Rate=FN/ (FN+TP)
True Acceptance Rate =1- False Reject Rate (18)

B. GABOR FILTERS

The character that an adjustable Gabor filter take down & combined by means of the original vein pictures were used in this work. The features, which were recognized as one of the image's channels, were fed into the network for validation and training. Since DL needs a lot of samples to train a robust weight after numerous repetitions, Gabor features were introduced. On the other hand, for the CASIA vein database, only 1200 photos (200 individual's × 3 sheets × 2 regularity spectra) may be employed for guidance under a good allocation of data. Since there wasn't as much data as in other sectors, the Gabor character is used to improve the original picture character without throwing off the data set's equilibrium. After that, ROC curves were created for comparison**.** In Figure 9, the acknowledgment rate under 850 nm and 940 nm light with Gabor character added is represented by the red and blue appearance, and the rate of recognition under 850 nm and 940 nm light without Gabor features is represented by the brown and yellow lines. It can be seen that the recognition rate under 940 nm light was higher than that under 850 nm light, and that the addition of the Gabor feature greatly increased the recognition rate of the two frequency bands.

REDVET - Revista electrónica de Veterinaria - ISSN 1695-7504
Vol 25, No. 1S (2024)
http://www.veterinaria.org
Article Received: Revised: Accepted:

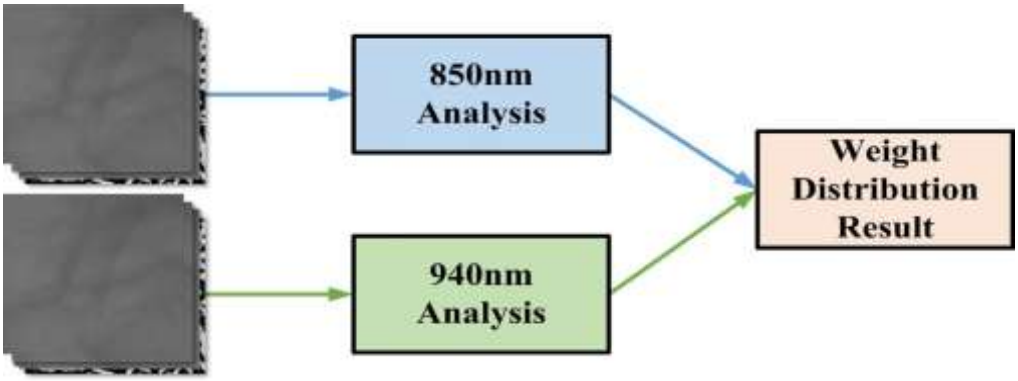

FIGURE 8. The system of weight choosing is weighted.

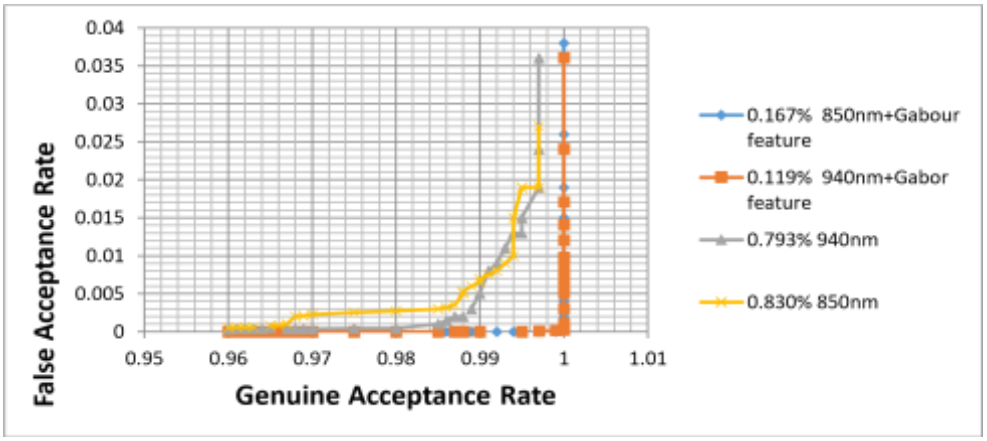

FIGURE 9. ROC curve with additional Gabor features.

C. THE METHOD FOR SELECTING WEIGHT

In this work, vein data obtained just at 850 nm and 940 nm frequencies was obtained from the CASIA collection. The proportional choosing technique that has been suggested has the potential to efficiently identify the optimal wavelength for users. As a result, the pictures for the 850nm and 940nm frequency bands were analyzed using a score fusion process, which gave the higher-quality band a higher weight. The weight choice procedure offers a more reliable verification method by efficiently integrating the data from frequency as well bands, as illustrated in Fig. 10.

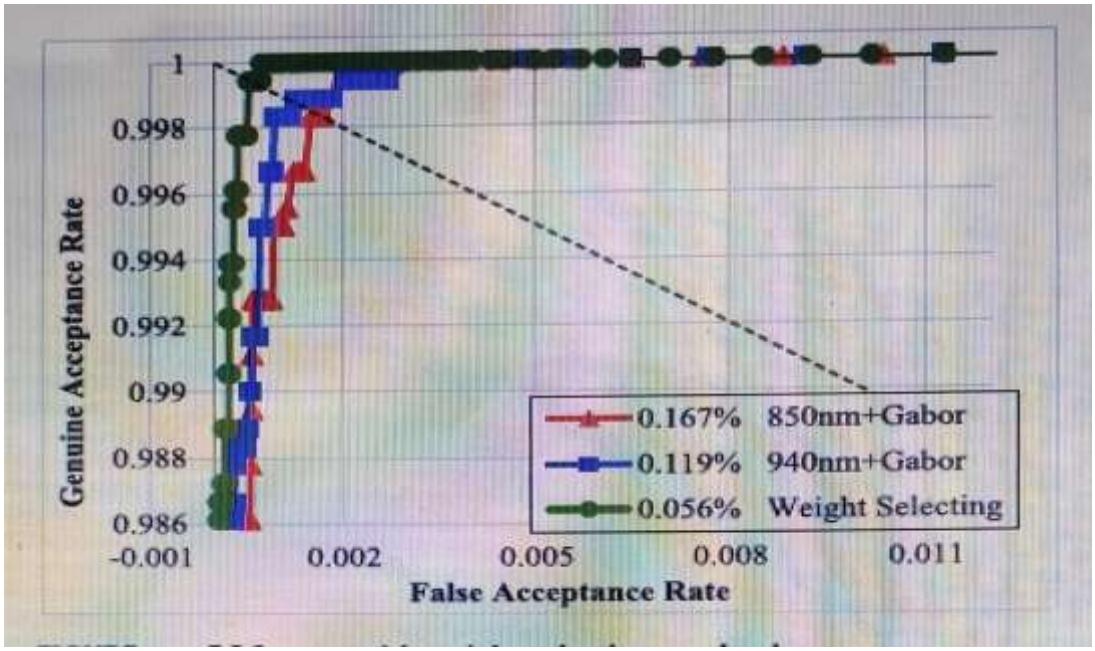

FIGURE 10. ROC curve includes a system for weight selection.

REDVET - Revista electrónica de Veterinaria - ISSN 1695-7504
Vol 25, No. 1S (2024)
http://www.veterinaria.org
Article Received: Revised: Accepted:

D. **CONSIDERATION WITH CONNECTED WORKS**

This paper conducted a comparison between the recommended methods and those found in previous papers using the same test conditions as those displayed in Table 3.It is separated into two categories: DL-based techniques and conventional CV procedures. The CV-based technique's EER was lower than the DL-based algorithm's since it may be adjusted using predetermined parameters to lessen the EER under particular devices and frequency circumstances. Achieving the same performance in various locations or on various devices is more challenging, though. Due to the growing number of users, some CV-based algorithms may have had a higher error rate than those studied in this research since they employed incomplete databases for comparison. Studies that employed deep learning (DL) for finger vein recognition with comparable sample features has been added for instance, while there have been few studies utilizing DL for palm vein recognition. Additionally, thin-layer DL network architecture for palm vein detection was established in this work. Our approach includes fewer characteristics than existing vein-related frameworks, such as MobileNetV2 [29], which are primarily utilized for embedding devices. As seen in Fig. 11, this also made it possible for the effort to carry out upcoming practical applications without the technology constraints that come with mobile devices and computational platforms at the edge.

The outcomes acquired from the PUT Vein Dataset [9], comprising 1200 photos with a wavelength of 880 nm and a size of 1280 × 960 pixels, are displayed in Table 4. There is just one picture to be tested and one to serve as training in the FYO collection. However, the current work suggests a third loss strategy that requires at least two images for successful training; as a result, we make use of the PUT dataset.

TABLE 3. Analyzing the EER confirmation success percentages of different methods.

Method	Year	Users	EER (%)
CV(Handcrafted)Method –Based			
NMRT[7]	2011	200	0.5100
Hessian phase[7]	2011	200	0.4300
Mutual foreground LBP[1]	2014	100	0.2670
Root SIFT[19]	2014	100	0.9960
Feature-level fusion[33]	2015	100	0.1600
Adaptive 2D Gabor filter[27]	2017	200	0.1200
CS-LBP[34]	2018	200	2.6100
HDPLS[12]	2019	100	0.0292
TERRM[4]	2020	200	4.2800
DL Method-Based			
ResNet01[36]	2018	200	6.1620
PVSNet[20]	2019	200	3.7100
MobileNetV2[29]	2019	200	5.9970
U-Net[50]	2020	100	0.47
DenseNet161[35]	2020	200	1.0540
CNN+Bayesian[51]	2021	100	0.0683
GPWLD[52]	2021	100	0.24
Proposed-850nm			0.1670
Proposed-940nm	2020	200	0.1190
Proposed-weight selecting			0.0456

#Parameter

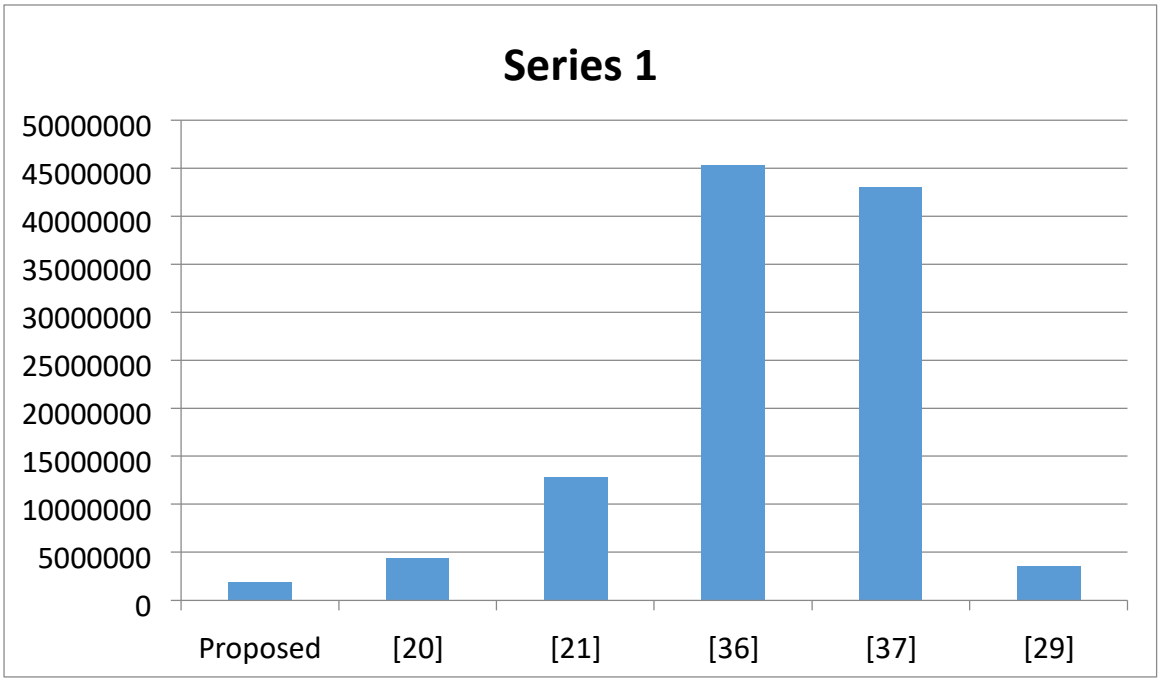

FIGURE 11. Analysis of the number of network parameters in comparison.

TABLE 4. Analysis among the PUT vein dataset's EER for various approaches.

Method	Year	Users	EER (%)
2D Correlation[38]	2011	100	1.10
Improved SIFT[39]	2017	100	1.08
Gradient-based 2D Gabor[40]	2019	100	1.60
Wave Atom Transform[41]	2020	100	0
MWCDE[42]	2020	100	0.62
MSDRA[43]	2021	100	0.791
Proposed-880nm	2020	100	0

The experimental findings show that the proposed method performs better than the other methods. Compared to the three earlier approaches, it is more successful [40]–[45]. The suggested approach outperforms the alternative approaches; as does the wave form particle transform [43]. We modify the size of the input picture to 320 × 320 × 4 in the PUT Vein Information set, that takes into consideration the GPU's instruction capacity and lessens the impact of deformation resulting from image resizing, in order to further investigate the practical performance between the technique provided in [43] and the suggested approach. In this work, a pair of convolution layers having widths of 32 and 64 and the ReLU activation function is added to the CNN. The path of the first level of convolution is 2×2.

5. CONCLUSION

Recent years have seen a significant increase in the development of vein-based identity identification, which has proven to be a dependable and efficient recognition technique. Nonetheless, a number of issues with the DL-based approach still need to be resolved. In light of this, the study suggested a comprehensive, lightweight system that successfully addressed the majority of issues with earlier systems. Following palm image input, the ROI positioning was able to withstand some rotation and displacement, which decreased usercaused system mistakes while preserving sanitary contactless capture.
Furthermore, a less complex system for palm veins was utilized, utilizing less parameter than persons found in previous research.
During network training, the input layer was fused, and the CNN network was trained to identify comparable features in different images using three-tuple loss function and Gabor characteristics. Even in situations where there is not enough data in the public database, it can still successfully train the CNN network. Furthermore, the mass selection technique improved the dualspectrum adaptability of the system by determining an excellent example. The results show that the recommended network framework needed fewer variables and had an improved failure rate of 0.0456%.

REFERENCES

1. W. Kang and Q. Wu, ``Contactless palm vein recognition using a mutual foreground-based local binary pattern," *IEEE Trans. Inf. Forensics Security*, vol. 9, no. 11, pp. 1974_1985, Nov. 2014.

2. C.-H. Hsia, J.-S. Chiang, and C.-Y. Lin, ``A face detection method for illumination variant condition," *Scientia Iranica*, vol. 22, no. 6,pp. 2081_2091, 2015.
3. D. Menotti, G. Chiachia, A. Pinto, W. R. Schwartz, H. Pedrini, A. X. Falcao, and A. Rocha, ``Deep representations for iris, face, an fingerprint spoofing detection," *IEEE Trans. Inf. Forensics Security*,vol. 10, no. 4, pp. 864_879, Apr. 2015.
4. S. Cho, B.-S. Oh, K.-A. Toh, and Z. Lin, ``Extraction and cross-matching of palm-vein and palm print from the RGB and the NIR spectrums for identity verification," *IEEE Access*, vol. 8, pp. 4005_4021, 2020.
5. C.-H. Hsia, ``New verification strategy for finger-vein recognition system," *IEEE Sensors J.*, vol. 18, no. 2, pp. 790_797, Jan. 2018.
6. C.-H. Hsia, ``Improved finger-vein pattern method using wavelet-based for real-time personal identification system," *J. Imag. Sci. Technol.*, vol. 26, no. 3, p. 30402, 2018.
7. Y. Zhou and A. Kumar, ``Human identification using palm-vein images,"*IEEE Trans. Inf. Forensics Security*, vol. 6, no. 4, pp. 1259_1274,Dec. 2011.
8. F. Liu, S. Jiang, B. Kang, and T. Hou, ``A recognition system for partiallyoccluded dorsal hand vein using improved biometric graph matching,"*IEEE Access*, vol. 8, pp. 74525_74534, 2020.
9. O. Toygar, F. O. Babalola, and Y. Bitirim, ``FYO: A novel multimodal veindatabase with palmar, dorsal and wrist biometrics," *IEEE Access*, vol. 8,pp. 82461_82470, 2020.
10. M. Zhou, L. Lin, M. Wang, X. Li, and G. Li, ``Infiuence of water on noninvasive hemoglobin measurement by dynamic spectrum," *Anal. Methods*, vol. 5, no. 18, pp. 4660_4665, 2013.
11. J.-D. Wu and S.-H. Ye, ``Driver identification using finger-vein patterns with Radon transform and neural network," *Expert Syst. Appl.*, vol. 36,no. 3, pp. 5793_5799, Apr. 2009.
12. W.Wu, S. J. Elliott, S. Lin, andW. Yuan, ``Low-cost biometric recognition system based on NIR palm vein image," *IET Biometrics*, vol. 8, no. 3,pp. 206_214, May 2019.
13. F. O. Babalola, Y. Bitirim, and Ö. Toygar, ``Palm vein recognition throughfusion of texture-based and CNN-based methods," *Signal, Image Video Process.*, vol. 15, pp. 1_8, Apr. 2020.
14. H. Zhang, C. Tang, A.W.-K. Kong, and N. Craft, ``Matching vein patterns from color images for forensic investigation," in *Proc. IEEE 5th Int. Conf.Biometrics, Theory, Appl. Syst. (BTAS)*, Sep. 2012, pp. 77_84.
15. N. Miura, A. Nagasaka, and T. Miyatake, ``Extraction of finger-vein patterns using maximum curvature points in image profiles," *IEICE Trans.Inf. Syst.*, vol. 90, no. 8, pp. 1185_1194, Aug. 2007.
16. L. Mirmohamadsadeghi and A. Drygajlo, ``Palm vein recognition with local binary patterns and local derivative patterns," in *Proc. Int. Joint Conf.*
17. *Biometrics (IJCB)*, Washington, DC, USA, Oct. 2011, pp. 1_6.
18. E. C. Lee, H. C. Lee, and K. R. Park, ``Finger vein recognition using minutiabased alignment and local binary pattern-based feature extraction," *Int. J. Imag. Syst. Technol.*, vol. 19, no. 3, pp. 179_186, 2009.
19. X. Li, S. Guo, F. Gao, and Y. Li, ``Vein pattern recognitions by moment invariants," in *Proc. 1st Int. Conf. Bioinf. Biomed. Eng.*, Wuhan, China, Jul. 2007, pp. 612_615.
20. W. Kang, Y. Liu, Q.Wu, and X. Yue, ``Contact-free palm-vein recognition based on local invariant features," *PLoS ONE*, vol. 9, no. 5, pp. 1_12, 2014.
21. D. Thapar, G. Jaswal, A. Nigam, and V. Kanhangad, ``PVSNet: Palm vein authentication Siamese network trained using triplet loss and adaptive hard mining by learning enforced domain specific features," in *Proc. IEEE 5th Int.*
22. *Conf. Identity, Secur., Behav. Anal. (ISBA)*, Hyderabad, India, Jan. 2019, pp. 1_8. [21] R. Das, E. Piciucco, E. Maiorana, and P. Campisi, ``Convolutional neural network for finger-vein-based biometric identification," *IEEE Trans. Inf. Forensics Security*, vol. 14, no. 2, pp. 360_373, 2019.
23. Y. Fang, Q. Wu, and W. Kang, ``A novel finger vein verification system based on two-stream convolutional network learning," *Neurocomputing*, vol. 290, pp. 100_107, May 2018.
24. C.-H. Hsia and C.-F. Lai, ``Embedded vein recognition system with wavelet domain," *Sensors Mater.*, vol. 32, no. 10, pp. 3221_3234, 2020.
25. R. Mehrotra, K. R. Namuduri, and N. Ranganathan, ``Gabor filterbased edge detection," *Pattern Recognit.*, vol. 25, no. 12, pp. 1479_1494,Dec. 1992. [25] J.-C. Lee, C.-H. Lee, C.-B. Hsu, P.-Y.Kuei, and K.-C. Chang, ``Dorsal hand vein recognition based on 2D Gabor filters," *Imag. Sci. J.*, vol. 62, no. 3,pp. 127_138, 2014.
26. [26] W.-Y. Han and J.-C. Lee, ``Palm vein recognition using adaptive Gabor filter," *Expert Syst. Appl.*, vol. 39, no. 18, pp. 13225_13234, Dec. 2012. [27] X. Ma, X. Jing, H. Huang, Y. Cui, and J. Mu, ``Palm vein recognition scheme based on an adaptive Gabor filter," *IET Biometrics*, vol. 6, no. 5, pp. 325_333, 2017.
27. O. Russakovsky, J. Deng, H. Su, J. Krause, S. Satheesh, S. Ma, Z. Huang, A. Karpathy, A. Khosla, M. Bernstein, A. C. Berg, and L. Fei-Fei, ``ImageNet large scale visual recognition challenge," 2014, *arXiv:1409.0575*.
28. M. Sandler, A. Howard, M. Zhu, A. Zhmoginov, and L.-C. Chen, ``MobileNetV2: Inverted residuals and linear bottlenecks," in *Proc. IEEE/CVF Conf. Comput. Vis. Pattern Recognit.*, Jun. 2018, pp. 4510_4520.
29. K. Simonyan and A. Zisserman, ``Very deep convolutional networks for large-scale image recognition," 2014, *arXiv:1409.1556*.

30. S. Tang, S. Zhou,W. Kang, Q. Wu, and F. Deng, ``Finger vein verification using a Siamese CNN," *IET Biometrics*, vol. 8, no. 5, pp. 306_315, Sep. 2019. [32] *CASIA Palm Image Database*. Accessed: Jul. 15, 2018. [Online]. Available: https://biometrics.idealtest.org/dbDetailForUser.do?id=5
31. X. Yan, W. Kang, F. Deng, and Q. Wu, ``Palm vein recognition based on multi-sampling and feature-level fusion," *Neurocomputing*, vol. 151, pp. 798_807, Mar. 2015.
32. S. Bhilare, G. Jaswal, V. Kanhangad, and A. Nigam, ``Single-sensor handvein multimodal biometric recognition using multiscale deep pyramidal approach," *Mach. Vis. Appl.*, vol. 29, no. 8, pp. 1269_1286, Nov. 2018.
33. K. J. Noh, J. Choi, J. S. Hong, and K. R. Park, ``Finger-vein recognition based on densely connected convolutional network using score-level fusion with shape and texture images," *IEEE Access*, vol. 8, pp. 96748_96766,2020.
34. W. Kim, J. M. Song, and K. R. Park, ``Multimodal biometric recognition based on convolutional neural network by the fusion of finger-vein and finger shape using near-infrared (NIR) camera sensor," *Sensors*, vol. 18, no. 7, p. 2296, 2018.
35. E. Jalilian and A. Uhl, ``Finger-vein recognition using deep fully convolutional neural semantic segmentation networks: The impact of training data," in *Proc. IEEE Int. Workshop Inf. Forensics Secur.*, Dec. 2018, pp. 1_8. [38] R. Kabacinski and K. Kowalski, ``Vein pattern database and benchmark results," *Electron. Lett.*, vol. 47, no. 20, pp. 1127_1128, 2011.
36. [39] G. Wang and J. Wang, ``SIFT based vein recognition models: Analysis and improvement," *Comput. Math. Methods Med.*, vol. 2017, pp. 1_14, Jun. 2017. [40] S. Bharathi and R. Sudhakar, ``Biometric recognition using finger and palm vein images," *Soft Comput.*, vol. 23, no. 6, pp. 1843_1855, Mar. 2019.
37. F. Ahmad, L.-M. Cheng, and A. Khan, ``Lightweight and privacypreserving template generation for palm-vein-based human recognition," *IEEE Trans. Inf. Forensics Security*, vol. 15, pp. 184_194, 2020.
38. G. Wang, C. Sun, and A. Sowmya, ``Multi-weighted co-occurrence descriptor encoding for vein recognition," *IEEE Trans. Inf. Forensics Security*, vol. 15, pp. 375_390, 2020.
39. Z. Pan, J. Wang, G. Wang, and J. Zhu, ``Multi-scale deep representation aggregation for vein recognition," *IEEE Trans. Inf. Forensics Security*, vol. 16, pp. 1_15, 2021.
40. H. Wan, L. Chen, H. Song, and J. Yang, ``Dorsal hand vein recognition based on convolutional neural networks," in *Proc. IEEE Int. Conf. Bioinf. Biomed. (BIBM)*, Nov. 2017, pp. 1215_1221.
41. C.-H. Hsia, J.-M. Guo, and C.-S. Wu, ``Finger-vein recognition based on parametric-oriented corrections," *Multimedia Tools Appl.*, vol. 76, no. 23, pp. 25179_25196, Dec. 2017.
42. T. E. Boult, ``PICO: Privacy through invertible cryptographic obscuration," in *Proc. Comput. Vis. Interact. Intell. Environ. (CVIIE)*, Nov. 2005, pp. 27_38.
43. V. G. Moshnyaga, J. Shioyama, and K. Hashimoto, ``A camera-based approach to prevent fingerprint hacking," in *Proc. IEEE Int. Workshop Signal Process. Syst.*, Oct. 2018, pp. 235_240.
44. K. Shaheed, H. Liu, G. Yang, I. Qureshi, J. Gou, and Y. Yin, ``A systematic review of finger vein recognition techniques," *Information*, vol. 9, no. 9,p. 213, Aug. 2018.
45. L.-C. Chen, Y. Zhu, G. Papandreou, F. Schroff, and H. Adam, ``Encoderdecoder with atrous separable convolution for semantic image segmentation," in *Proc. Eur. Conf. Comput. Vis.*, Munich, Germany, 2018, pp. 833_851.
46. P. Wang and H. Qin, ``Palm-vein verification based on U-Net," *IOP Conf. Mater. Sci. Eng.*, vol. 806, Apr. 2020, Art. no. 012043.
47. M. I. Obayya, M. El-Ghandour, and F. Alrowais, ``Contactless palm vein authentication using deep learning with Bayesian optimization," *IEEE Access*, vol. 9, pp. 1940_1957, 2021.
48. M. El-Ghandour, M. I. Obayya, B. Yousef, and N. F. Areed, ``Palmvein recognition using block-based WLD histogram of Gabor feature maps and deep neural network with Bayesian optimization," *IEEE Access*, vol. 9, pp. 97337_97353, 2021.